Symbiotic Self-Assembly Strategy toward Lipid-Encased Cross-Linked Polymer Nanoparticles for Efficient Gene Silencing

A Symbiotic Self-assembly Strategy towards Lipid-encased Crosslinked Polymer Nanoparticle for Efficient Gene Silencing

Kingshuk Dutta,[a] Davide Bochicchio,[b] Alexander E. Ribbe,[c] Dominique Alfandari,[d,e,f] Jesse Mager,[d,e,f] Giovanni M. Pavan,[b,g] and S. Thayumanavan[a,e,f]*

[a]Department of Chemistry, [c]Department of Polymer Science and Engineering, [d]Department of Veterinary and Animal Sciences, [e]Molecular and Cellular Biology Program, and [f]The Center for Bioactive Delivery- Institute for Applied Life Sciences, and University of Massachusetts, Amherst, Massachusetts 01003, United States

[b]Department of Innovative Technologies, University of Applied Sciences and Arts of Southern Switzerland, CH-6928 Manno, Switzerland, and [g]Department of Applied Science and Technology, Politecnico di Torino, Corso Duca degli Abruzzi 24, 10129 Torino, Italy

ABSTRACT: A novel 'symbiotic self-assembly' strategy that integrates the advantages of biocompatible lipids with a structurally robust polymer to efficiently encapsulate and deliver siRNAs is reported. The assembly process is considered to be symbiotic, because none of the assembling components are capable of self-assembly, but can form well-defined nanostructures in the presence of others. The conditions of the self-assembly process are simple, but have been chosen such that it offers the ability to arrive at a system that is non-cationic for mitigating carrier-based cytotoxicity, efficiently encapsulate siRNA to minimize cargo loss, effectively camouflaged to protect the siRNA from nuclease degradation, and efficiently escape the endosome to cause gene knockdown. The lipid-siRNA-polymer (L-siP) nanoassembly formation and its disassembly in the presence of an intracellular trigger have been extensively characterized experimentally and through computational modeling. The complexes have been evaluated for delivery of four different

siRNA molecules in three different cell lines, where an efficient gene knock-down is demonstrated. The reported generalized strategy has the potential to make an impact in the development of a safe and effective delivery agent for RNAi mediated gene therapy that holds the promise of targeting several hard-to-cure diseases.

Keywords: siRNA delivery, symbiotic self-assembly, random co-polymer, noncationic delivery agent, zwitterionic lipids, DOPE, gene silencing, eGFP, PLK1, MDR1

1. INTRODUCTION

Self-assembly that relies on non-covalent intermolecular interactions, comprising single or multi-component molecular building blocks, plays a fundamentally important role in many biological processes and in the development of novel functional materials.[1-2] However, designing and assembling multiple molecular entities to generate a predictable and controlled supramolecular assembly have considerable challenges; but if achieved, this can propel the design of materials with functional capabilities that are currently not attainable. With this in mind, we have designed a new three-component self-assembling system, where the parts are interdependent in the formation of the nanoassembly. In addition to demonstrating the formation and the characterization of such an assembly, the utility of such a nanostructure in addressing current toxicity and cellular delivery challenges involving small interfering RNA (siRNA) molecules has been investigated.

Although discovery of siRNA, a potential gene silencing agent, has created attractive opportunities targeting a wide array of diseases,[3-5] RNAi technology has produced only one drug approved for clinical use.[6] Poor cellular internalization, serum instability, rapid clearance, severe cytotoxicity and potential immunological flare-ups have been identified as the critical barriers for such promising technology.[7-12] Potential solutions like, chemically modified siRNAs and viral vectors have yet to overcome issues owing to cytotoxicity, stability, immunogenicity and reduced silencing ability upon structural modifications.[7, 13-14] Interestingly, non-viral approaches, based on electrostatic complexation of nucleic acids using cationic lipids, peptides, nanoparticles, or polymers, have the potential to resolve the major reported issues.[15-20] However, the key obstacle in these carrier-based delivery systems is the adverse side effects originated from the cationic

charge mediated alteration in membrane potentials of cellular organelles and non-specific interactions with negatively charged serum proteins.[13, 21-22]

To address this, two interesting approaches, *viz.* charge-masking strategies[23-24] and spherical nucleic acids[25] have been reported wherein cationic charges are masked and negatively charged nucleic acids are decorated on surfaces, respectively. In addition to the non-cationic surface display, the degradable cationic blocks offer opportunities to mitigate toxicity issues associated with cationic polymers as well.[26-29] Mimicking viral mechanism of cellular entry, another polymeric delivery agent, virus-inspired polymer for endosomal release, is developed with a hydrophilic cationic block and an endosomolytic peptide displayed only under acidic pH.[30] In a significant departure from the conventional approaches, direct decoration of a high density of nucleic acids themselves as surface functionalities on nanoparticles and polymers have produced negatively charged nanostructures with good cellular internalization and gene silencing capabilities.[25, 31] Natural green tea catechin condensed siRNA-cationic polymer nanoparticles and fluorinated oligoethylenimine nanocomplexes have also shown encouraging outcomes for siRNA delivery.[32-33] Despite these advances, there still exists a need for RNAi-based therapeutic approaches that would retain the key advantages of non-viral carriers, while mitigating their shortcomings.

Inspired by this, we envisaged that a possible solution to all these delicate and overwhelming challenges would be a noncationic approach wherein the cationic charge is irreversibly removed after encapsulation of siRNA without compromising stability and activity of the nucleic acid. To this end, we designed a unique and well-defined 'symbiotic self-assembly' approach to efficiently self-assemble a polymer, lipids, and the nucleic acid to form stable lipid decorated siRNA-polymer (L-siP) nanoassemblies (**Scheme 1**). We term this as symbiotic self-

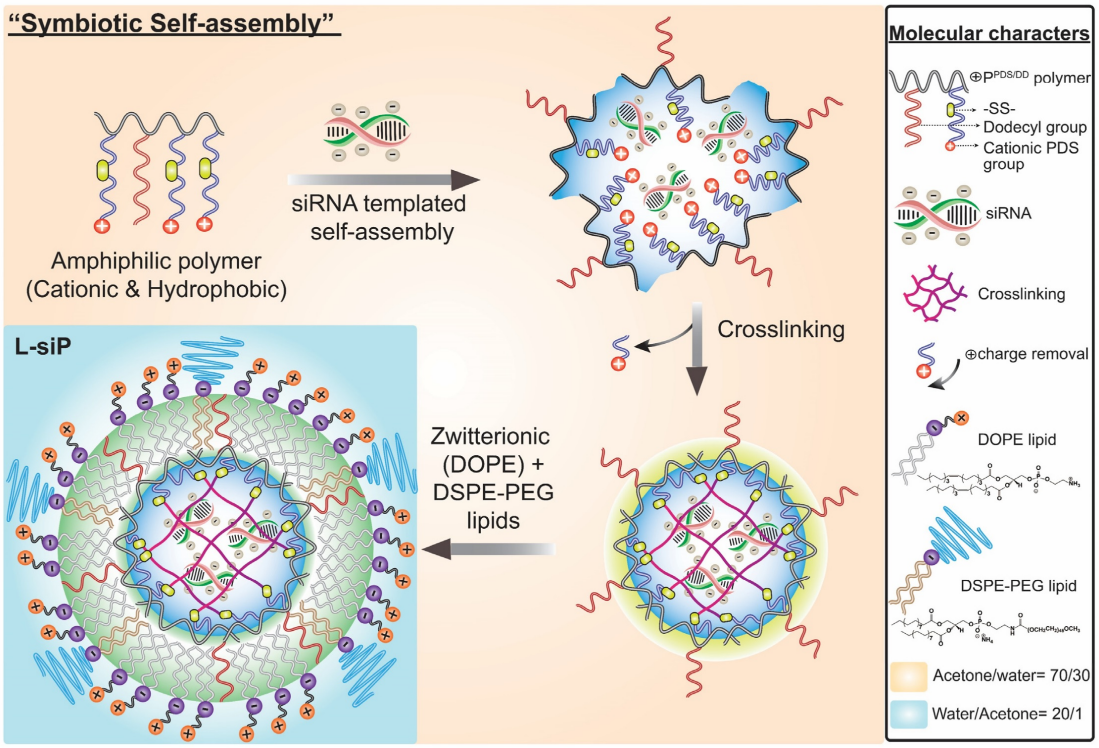

Scheme 1. Symbiotic self-assembly strategy to construct L-siP nanoassembly and its key molecular components.

assembly, because none of these three components would form the nanostructures by themselves under the required conditions, but they produce well-defined assemblies when brought together in a sequence. We outline the design hypothesis, self-assembly, and their utility in effectively delivering siRNA molecules inside cells, using four different siRNAs in different cell lines. The system has been designed such that: (*i*) the high binding affinity results in efficient capture of siRNAs inside the assemblies; (*ii*) although electrostatics is utilized to capture the siRNAs, the residual assembly is non-cationic due to an *in situ* crosslinking protocol that removes the cationic charge on the polymer, yet incarcerates the siRNA; (*iii*) the surface charge of the assemblies is non-cationic; and (*iv*) the siRNA can be released using a trigger that corresponds to the operational environment of the cargo.

2. EXPERIMENTAL SECTION

2.1. Materials & Characterizations

Materials and characterization techniques are described in Supporting Information file.

2.2. Synthesis of Random Co-polymer for Complexation with siRNA

2.2.1. Synthesis of p(PDSMA-co-DodecylMA) Polymer ($P^{PDS/DD}$)

Pyridyl disulfide ethyl methacrylate (PDSMA) was synthesized using previously reported procedure.[34] Reversible Addition-Fragmentation chain Transfer (RAFT) polymerization was utilized to synthesize p(PDSMA-co-DodecylMA) Polymer. In a typical procedure, PDSMA (0.903 g, 3.5 mmol), dodecyl methacrylate and chain transfer agent 4-cyano-4-(phenylcarbonothioylthio)pentanoic acid were taken in a 25 mL Schlenk flask and dissolved in 2 mL dry THF. To this mixture, 1.1 mg (0.007 mmol) AIBN, dissolved in 1 mL dry THF, was added. The solution was mixed for 5 min, the flask was subjected to three freeze-pump-thaw cycles and purged with argon. Finally, the sealed flask was transferred to a preheated oil-bath and the polymerization was carried out at 70 °C for 24 h. After that, the Schlenk flask was cooled down to quench the reaction and THF was evaporated. The reaction mixture was purified by precipitating in diethyl ether for three times and finally dried in vacuo for overnight at room temperature. Yield: 78%, GPC (THF) Mn: 14.5 kDa, Đ: 1.3; 1H NMR (400 MHz, CDCl3): δ ppm 4.24−4.09, 3.87, 3.65−3.53, 3.37, 2.95-2.90, 1.93-1.84, 1.04-0.89; 13C NMR (100 MHz, CDCl3): δ ppm 177.4, 177.07, 176.34, 159.69, 159.56, 159.5, 149.87, 137.31, 121.07, 120.01, 119.96, 62.84, 54.47, 45.34, 45.28, 45.00, 32.06, 31.71, 29.80, 29.50, 29.18, 25.41, 22.83, 14.25, 11.56.

2.2.2. Synthesis of Cationic-PDS-Dodecyl Polymer ($\oplus P^{PDS/DD}$)

In a 20 mL glass vial, 0.75 g of PPDS/DD polymer was weighed and dissolved in 5 mL DCM. The solution was cooled in ice for 10 min and after that methyl trifluoromethanesulfonate (0.73 g, 4.4 mmol) was added to it dropwise. The mixture was stirred at 4 °C overnight, the solvent was dried and precipitated in diethyl ether three times to purify. The polymer was dried overnight in vacuo at room temperature. Yield: 75%, calculated Mn: ~22 kDa; 1H NMR (400 MHz, CDCl3): δ ppm 4.24−4.09, 3.87, 3.65−3.53, 3.37, 2.95-2.90, 1.93-1.84, 1.04-0.89; 13C NMR (100 MHz, CDCl3): δ ppm 177.33, 159.3, 159.13, 147.57, 144.35, 125.51, 124.03, 122.05, 115.7, 62.51, 45.7, 45.13, 44.86, 37.1, 36.97, 31.73, 31.35, 29.43, 22.4, 19.08, 16.95, 13.02.

2.3. Study of siRNA Encapsulation with Varying Dosages of $\oplus P^{PDS/DD}$ Polymer (at Different N/P Ratios)

2.3.1. Preparation of L-siP Nanoassembly Without Crosslinking

To study the effect of N/P ratio on complexation, two different sets of solutions were prepared containing siRNA and $\oplus P^{PDS/DD}$ in a mixed solvent system (acetone:water=70:30). In first set, a fixed amount of siRNA (2 µg) was dosed in acetone/water solvent mixtures (70:30) to get 50 µL identical solutions. In another set, different amounts $\oplus P^{PDS/DD}$ polymer solution (2 mg/mL in acetone:water= 70:30) were diluted with same mixed solvent system to achieve another 50 µL solutions. Afterwards, the polymer solutions were added to the fixed amount siRNA solutions (containing 2 µg siRNA) to finally achieve N/P ratios of 5, 7.5, 10, 15, 20 and 25. All these mixed solutions were incubated for 2h in an orbital shaker at 20 °C to facilitate complexation. Meanwhile, mixed lipid solutions were prepared in 2 mL water containing 20% wt./wt. DOPE & 10 mol%

DSPE-PEG (based on $\oplus P^{PDS/DD}$ polymer) and stirred for 30 min. Next, each of 100 µL nanoassembly solutions, after 2 h complexation period, was added to an aqueous pool of lipid mixture and stirred for 3 h at 20 °C. In this step, the glass vials were kept open to facilitate the evaporation of organic solvents and maturation/hardening of the nanoassemblies. Finally, the solutions were filtered through Amicon Ultra Centrifugal Filters MWCO 10 kDa to remove remaining organic solvents, purify and concentrate the solutions. The final volume of L-siP nanoassembly solutions was adjusted to 100 µL with nuclease-free deionized water.

2.3.2. Preparation of L-siP Nanoassembly With Crosslinking

Crosslinking of L-siP nanoassemblies were achieved by introducing DTT solutions after the complexation step. Different amounts of DTT (0.1, 0.25, 0.5, 1 and 2 equivalents with respect to PDS moiety in $\oplus P^{PDS/DD}$ polymer) dissolved in acetone/water (70:30) mix solvent were added to the siRNA-polymer mixtures after 2 h complexation step. Each solution was incubated in an orbital shaker at 20 °C for another 2 h. After that all solutions were subjected to lipid locating step.

2.4. Agarose-gel Retardation Assay for Proof of Complexation & siRNA Release

2.4.1. Encapsulation Study

20 µL samples (with different N/P ratios and varying crosslinking) were mixed with 4 µL of gel loading buffer and loaded into 2% agarose gel made in TAE buffer containing EtBr. Samples were run in horizontal electrophoresis system at 110 V for 1 h and subjected to imaging analysis with NuGenius gel imager system (Syngene).

2.4.2. Release Study

20 µL sample was mixed with 1 µL Triton-x (0.1 g/mL) and sonicated for 5 min. Next, 250 mM glutathione solution was added to it and the pH was adjusted to ~7-8 with 1 N NaOH solution (final glutathione concentration was 10 mM). The mixture was incubated for 6 h at 37 °C and subjected to agarose gel electrophoresis and visualization method as described above.

2.5. MD-simulations: Modelling for Encapsulation & Release

Construction of coarse-grained (CG) models, simulation parameters, features of N/P 7.5 and 15 systems, DTT crosslinking, Construction of complete L-siP nanoassembly and release simulations of siRNA are described in detail in Supporting Information. Here, we have decided to use dsDNA as our CG models are based on the MARTINI force field, for which reliable dsDNA parameters are already available in literature. However, our choice is justified also by the fact that, at the level of precision of our CG models, the difference between dsDNA and siRNA is likely to be negligible, given the electrostatic nature of self-assembly in this system and the fact that the charges would be the same in molecules of same lengths.

2.6. Cell culture

HeLa (cervical cancer), DU 145 (prostate cancer) , MDA-MB-231 (mammary gland/breast cancer), NCI/ADR-RES (derived from the ovarian cell line OVCAR-8/Adriamycin (Doxorubicin or Dox) resistant, procured from NCI, Frederick), HeLa^{eGFP} and DU 145^{eGFP} (eGFP transfected) cell lines were cultured in 100 mm cell culture petri-dish containing Dulbecco's Modified Eagle Medium/Nutrient Mixture F-12 (DMEM/F12) in a humidified incubator with 5% CO2 at 37 °C. Culture media was supplemented with 10% fetal bovine serum (FBS), 1% L-glutamine and 1% antibiotic-antimycotic (100 units/mL of penicillin, 100 µg/mL of streptomycin, and 0.25 µg/mL of Amphotericin B).

2.7. Cellular Internalization, Endosomal Escape and L-siP Nanoassembly Stability Studies

Quantification of cellular uptake via confocal microscopy and flow cytometry, endocytosis mechanism, endosomal escape studies and stability of L-siP nanoassemblies in presence of RNase A and serum were discussed in detail in Supporting Information section.

2.8. Toxicity studies of L-siP nanoassemblies in HeLa/DU-145/MDA-MB-231 cell lines

2.8.1. AlamarBlue assay for cellular viability

HeLa, DU 145 and MDA-MB-231 cells were seeded (7.5×10^3 cells in 0.1 mL per well) into 96-well tissue culture plates and incubated at 37 °C. After 24 h, cell culture media was replaced with serum-free media containing L-siP nanoassemblies bearing different concentrations of negative control siRNA (25, 50, 100, 200 and 500 nM). Identical control crosslinked nanoassemblies devoid of any siRNA, L-siP(empty), were also tested for toxicity. Lipofectamine® RNAiMAX was complexed at different dosages (2, 5 and 10 μg/mL) with negative control siRNA (at 100 nM) and compared with other samples. After 24 h incubation, media was replaced with complete fresh one and incubated for another 2 days (72 h in total). After that cells were washed with PBS for three times and each well was treated with 100 μL 10% alamarBlue in complete media. Finally, cells were incubated for 1 h at 37 °C and solutions were transferred to black 96-well flat-bottomed plate for fluorescence measurement with SpectraMax® M5 microplate reader (excitation: 560 nm, emission: 590 nm).

2.8.2. LDH cytotoxicity assay for membrane damage studies

For LDH assay, all cells were incubated with L-siP nanoassembliess for 24 h and then subjected to Pierce LDH cytotoxicity assay.[35] 50 μL of media was collected from 96 well cell culture plate

and transferred to another 96 well plate. To that solution 50 µL LDH reaction mixture was added and incubated at room temperature for 30 min. Next, 50 µL stop solution was added to each well and subjected to absorbance measurements with SpectraMax® M5 microplate reader at 490 nm and 680 nm (cytotoxicity was calculated based on absorbance, $A = A_{490}-A_{680}$).

2.9. Gene silencing studies

2.9.1. Knockdown of GFP in GFP-transfected HeLa & DU-145 cell lines through flow cytometry & confocal microscopy

To study the gene silencing, GFP-transfected HeLa and DU-145 cells were plated in 12 well plate (5×10^4 cells in each well) and incubated for 24 h at 37 °C. After that cells were transfected with GFP-siRNA loaded L-siP nanoassemblies (50, 100 & 200 nM siRNA concentrations) and incubated for 24 h. Next, media was replaced with fresh one and incubated for another 24 h at 37 °C. Finally, cells were trypsinized, pelleted by centrifugation and washed two times with PBS followed by suspension in 500 µL PBS. Flow cytometry was performed with this cell suspension in a BD LSRFortessa™ instrument (excitation wavelength: 488 nm, FITC channel) to check the reduction in GFP fluorescence intensity. FlowJo version 10 software was used to analyze data and obtain fluorescence intensities of the samples.

For confocal microscopy analyses for GFP-silencing, 1×10^5 cells were plated in 35 mm glass-bottomed petri-dishes and incubated for 3 days at 37°C and 5% CO_2 incubator for proper adhesion. Afterwards cells were transfected with L-siP-GFP-siRNA nanoassemblies, incubated for 24 h, washed and subjected to further 24 h incubation before subjecting to washed three times with PBS buffer and incubated with L-siP nanoassemblies containing 100 nM cy3-siRNA in 1 mL serum-free media at 37 °C for 24 h. Next, the media was removed, washed three times with PBS and incubated with NucBlue™ Live ReadyProbes™ reagent in FBS containing media for 1 h to stain

cell nucleus. Live cell imaging was performed using Nikon Spinning Disk confocal microscope. All images were analyzed with Nikon NIS-Elements software.

2.9.2. Knockdown of PLK1 in MDA-MB-231 and MDR1 in NCI-ADR/RES cell lines through qPCR & western blot studies

1.5×10^5 cells were plated in 6 well tissue culture plate, incubated for 24 h at 37 °C- 5% CO_2 atmosphere and then transfected with L-siP nanoassemblies containing PLK1 and MDR1 siRNA (at 50 & 100 nM siRNA concentration) for MDA-MB-231 & NCI-ADR/RES cells, respectively. Control samples containing L-siP nanoassemblies without siRNA, untreated cells and only siRNA treated cells were subjected to similar conditions. After transfection (24 h), media was changed and incubated at 37 °C- 5% CO_2 atmosphere for another 24 h.

qPCR studies

Finally, cells were washed and total RNA was isolated by RNA extraction kit (High Pure RNA Isolation Kit, Roche) according to manufacturer's protocol. Isolated RNAs were checked for purity and concentrations by measuring absorbances at 260/280 nm.

Next, cDNA synthesis was performed with iScript cDNA synthesis kit (Bio-Rad Laboratories) from the isolated RNA. After that, RT-PCR was performed using the synthesized cDNA, PerfeCTa MultiPlex qPCR SuperMix (Low ROX) and Taqman probes for PLK1, MDR1 and control β-actin genes in Mx3005P qPCR System (Stratagene/Agilent). Target gene expression levels were normalized and reported as fold increase compared to β-actin using the ΔΔCT method.

Western blot analyses

To isolate total proteins, cells were washed with cold PBS buffer once and scraped to de-touch from the plate and transferred with cold PBS to an eppendorf tube. Afterwards, cells were

pelletized by centrifugation, washed with cold PBS twice to remove proteins from media. Next, RIPA lysis buffer containing protease/phosphatase inhibitor mix was added to the cell pellet keeping it in ice and incubated for 15 min, followed by 3×30 s sonication to ensure complete lysis of cells. Finally, lysed cells were centrifuged at 14000 rpm - 4 °C to collect soluble protein extracts and quantified with 660 nm protein assay.

Western blot analyses were performed to identify PLK1 and MDR1/P-gp protein levels in cells. Rabbit monoclonal antibodies (PLK1, MDR1/ABCB1 & β-Actin mAbs, Cell Signaling) were used to detect target proteins and loading control. HRP-linked anti-rabbit IgG was used as secondary antibody and proteins bands were detected by enhanced chemiluminescence (ECL) reagent (Luminol, coumaric acid and H_2O_2).

3. RESULTS AND DISCUSSION

The self-assembly process was envisioned in three key steps. First, a cationic amphiphilic polymer would be utilized to electrostatically capture the siRNA (**Scheme 1**, **Figure 1a-b**). Note that electrostatic interaction energy is governed by Coulomb's law ($E=q_1.q_2/4\pi\varepsilon_o\varepsilon r$), where ε represents the dielectric constant of the medium. In this case, the ionic interaction between the polymer and the siRNA can be significantly enhanced in low dielectric media. The hydrophobic alkyl chain in the amphiphilic random copolymer facilitates the complexation between the polymer and the siRNA in an organic-rich solvent medium, where the electrostatic interactions are expected to be strong. However, the medium is not completely non-aqueous, as polyelectrolyte interactions are entropically driven[36] and it is important to accommodate the critical counterion dissociation that facilitates the interaction between these two macromolecules. Second, while we utilize the cationic charge to bind the siRNA with high affinity, we are interested in eliminating the cationic

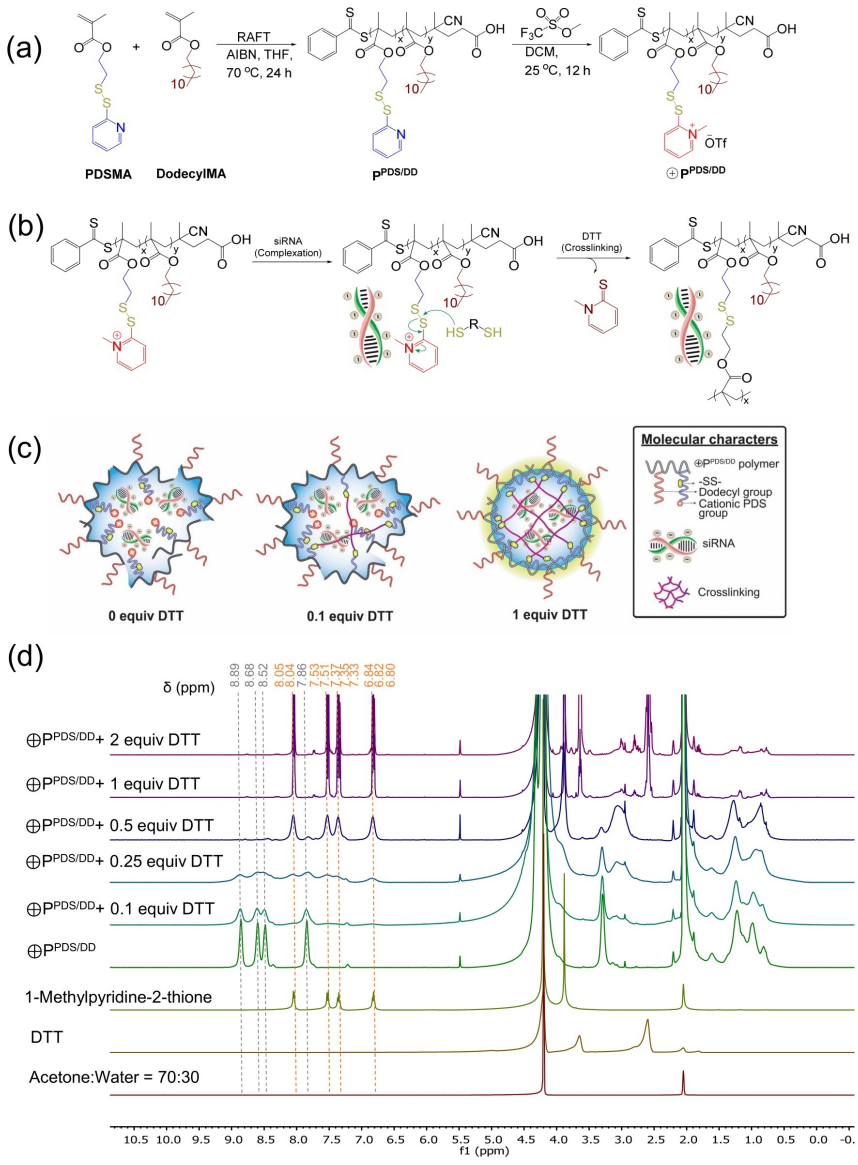

Figure 1. (a) Synthesis of p(PDSMA-co-DodecylMA) polymer ($P^{PDS/DD}$) and post-polymerization modification to install cationic charge yielding $\oplus P^{PDS/DD}$ polymer; (b) Reaction scheme for preparation of non-cationic L-siP nanoparticles via disulfide based crosslinking; (c) Schematic representation of differentially crosslinked polymer-siRNA assemblies; (d) ^{1}H NMR spectra of $\oplus P^{PDS/DD}$ polymer treated with different amounts of DTT for crosslinking in acetone:water (deuterated)= 70:30.

charge in the system since this has been implicated in many complications in non-viral carriers.[13, 21-22] Therefore, we utilize a cationic functional group that can be triggered to concurrently self-crosslink and release the cationic functionality (**Scheme 1**, **Figure 1b-c**). Such a process switches

the driving force for retaining the siRNA within the assembly, from an electrostatic one to a combination of physical incarceration (due to crosslinking) and solvophobic forces (due to the unfavorable organic-rich medium for the highly charged siRNA). Finally, the resultant complex from this process is relatively apolar with lipophilic alkyl chains on their surface; this complex therefore is not amenable for distribution in aqueous media. We utilize this incompatibility to achieve a hydrophobic force driven coating of charge-neutral lipids in aqueous medium. The concentration of the lipids in this step is such that it does not exhibit self-assembly by itself, but does so on the surface of the existing hydrophobic exterior of the polymer-siRNA complex. This symbiotic self-assembly, where the organization of each of these components into the assembly is dependent on the presence of other components in the system, is thus achieved in three convenient steps.

3.1. Synthesis, characterization and crosslinking study of cationic PDS-Dodecyl polymer ($\oplus$P$^{PDS/DD}$). To achieve the desired self-assembly, a cationic random co-polymer PDS-Dodecyl polymer ($\oplus$P$^{PDS/DD}$) was targeted (**Figure 1a**). This copolymer was synthesized via RAFT polymerization of pyridyl disulfide methacrylate and dodecyl methacrylate monomers (molar ratio 9:1, **Figure 1**, see **SI** for details) to obtain p(PDSMA-co-DodecylMA) polymer (P$^{PDS/DD}$; MW =14.5 kDa; Đ: 1.3). The nitrogens in the PDSMA side-chain were quantitatively methylated using methyl triflate to achieve the $\oplus$P$^{PDS/DD}$ polymer (**Figure 1**, **SI**). All polymers were characterized with ^{1}H, ^{13}C & ^{1}H-^{15}N NMR, GPC and FT-IR spectroscopy (see **SI** and **Figure S1-S5**). Methylation of the P$^{PDS/DD}$ polymer was confirmed from the chemical shift and integration of pyridinium ring protons in the final $\oplus$P$^{PDS/DD}$ polymer. To further confirm the synthesis of the $\oplus$P$^{PDS/DD}$ polymer, two-dimensional heteronuclear correlation NMR experiments (^{1}H-^{15}N HMBC, **Figure S3**) were performed with the synthesized polymers and 1-methylpyridine-2-thione

molecule, released after crosslinking with 1,4-dithiothreitol (DTT, reported in equivalents). A clear shift of ^{15}N NMR band for $\oplus P^{PDS/DD}$ polymer, in addition to appearance of a new correlation band corresponding to methylated nitrogen, confirms successful installation of cationic charge in the $\oplus P^{PDS/DD}$ polymer. Further, ^{1}H NMR spectra for differentially crosslinked samples in presence of different amounts of DTT showed the disappearance of the methylated-PDS units with the concurrent appearance of the peaks that correspond to the small molecule byproduct of the crosslinking reaction, N-methylpyridothione (**Figure 1d**). These experiments were carried with the polymer by itself without self-assembling the polymer through electrostatic complexation with siRNA, for characterization purposes. Note that complete crosslinking was achieved at 1 equiv DTT (2 times excess than required) which could be attributed to suppressed reactivity owing to steric barriers.

3.2. 'Symbiotic self-assembly' to create L-siP nanoassemblies. The first step of proposed self-assembly (**Scheme 1**) involves electrostatic complexation between $\oplus P^{PDS/DD}$ polymer with naked siRNA in acetone:water mixture (70:30 v/v). In addition to reducing the dielectric constant of the media[37] to facilitate greater Coulombic interaction, the choice of solvent mixture is also optimized for the solubility of both $\oplus P^{PDS/DD}$ polymer & siRNA. The amphiphilicity of $\oplus P^{PDS/DD}$ polymer, governed by the ratio of cationic PDS and dodecyl moieties, was also found to affect the solubility of such complexes. We found that 90:10 ratio polymer exhibited better solubility and complexation capability, compared to that of the initially attempted 70:30 ratio polymer. All subsequent complexation experiments were conducted with the 90:10 ratio polymer in the acetone:water co-solvent system. To further analyze whether the observed interaction between the polymer and the siRNA is indeed based on electrostatics, we conducted molecular dynamics (MD) simulations of a coarse-grained (CG) molecular model of this system (see **SI** for details about the model) in the

acetone:water 70:30 mixture. Simulations show that while the cationic polymers and the oligonucleotides are held together, removal of cationic charge in the polymer detaches the oligonucleotides from the polymer chain. This supports the idea that the self-assembly process is controlled by electrostatic interactions (see **SI**).

The next step in our self-assembly involves structurally reinforcing the complex through a chemical crosslinking reaction, which concurrently also releases the cationic charge from the polymer. This crosslinking step was executed using DTT, where the rapid thiol-disulfide exchange reaction between DTT and the methylated-PDS unit affords a thiol moiety on the polymer side chain, along with a stable small molecule byproduct, *viz.* *N*-methylpyridine-2-thione. The thiol moiety on the polymer chain can subsequently react with other methylated-PDS units within the complex to generate crosslinks. Note that this crosslinking step helps to shed positive charge, while also stitching the polymer chains to cage siRNA, thus preventing the loss of siRNA that is electrostatically encapsulated in the first step. More details on the effect of crosslinking density is provided in the next section.

Note that the complexation and crosslinking steps were conducted in an organic rich (acetone-water) media. In order for using this complex to deliver the siRNA molecule to cells, this complex must be in an aqueous media. To achieve this, the complex was coated with lipids in aqueous phase. Since the crosslinked polymer-siRNA complex was achieved in an organic solvent, we envisaged that the surface of the complex is apolar and would therefore be viable for coating with lipid molecules. Accordingly, we used a combination of a zwitterionic lipid (DOPE) and a PEGylated lipid (DSPE PEG-2000), because of their fusogenic and solubilization abilities respectively.[9,38-39] Briefly, a mixture of DOPE and DSPE PEG-2000 lipids was initially dissolved in water at a concentration much below their critical aggregation concentrations.[40] The crosslinked

polymer-siRNA nanoassembly was then added to the aqueous lipid mixture (water/organic=20, v/v) for the self-assembly of lipids on its surface (see **SI** for details) to produce the final lipid-

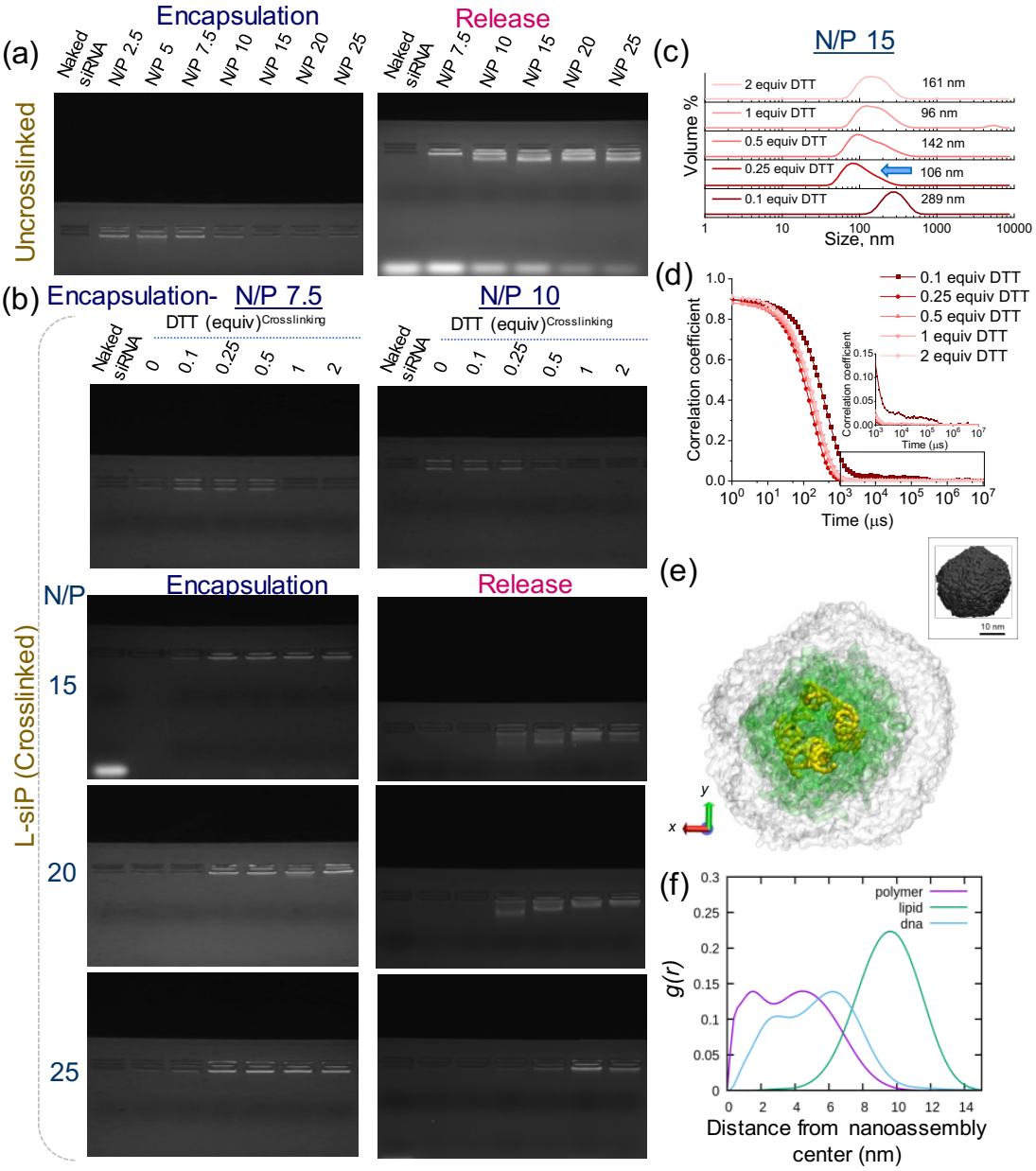

Figure 2. Effect of N/P ratio & cross-linking on encapsulation stability & siRNA release: (a) Variation of N/P for uncrosslinked particles; (b) Effect of variation of cross-linking measured by the DTT feed amount at higher N/P ratio on encapsulation & siRNA release; (c) DLS size distribution and (d) correlation diagram for N/P 15 nanoassemblies at different cross-linking; (e) Lipid coated nanoassembly constructed with CG-MD simulation: snapshot of the equilibrated L-siP$^{15/1}$ (cut in half on the major diameter to clearly see the interior). Polymer is shown in transparent green, the dsDNA in yellow and the polymer outer layer is transparent grey (inset: exterior of the NA, where lipids are shown in grey); (f) Radial distribution functions *g(r)* providing the relative probability to find polymer, dsDNA and lipids at various distances from the center of the nanoassembly.

polymer-siRNA (L-siP) nanoassembly (**Scheme 1)**. Interestingly, the overall self-assembly process is considered symbiotic, because the lipids are used at concentrations well below their CACs and yet it self-assembles on the surface of the polymer-siRNA complex, which in itself required functional complementarity for its formation.

3.3. Effect of N/P and crosslinking on complexation and triggered release of siRNA from L-siP. The relative ratio of complementary charges (N/P) is often used, with number of positively charged nitrogens (N) in the polymer to the number of negatively charged phosphate moieties (P) in the nucleic acid as the measure, to evaluate the complexation efficiency. To understand the effect of this ratio on complexation, we systematically varied the amount of polymer to investigate the construction of L-siP assemblies at different N/P ratios (**Figure 2**). All particles were coated with DOPE and PEG-lipids to make them hydrophilic and stable in aqueous medium. The siRNA encapsulation was evaluated with agarose gel retardation assay (**Figure 2a-b**). First, complexation was studied at different N/P ratios without any crosslinking. At low polymer concentrations (N/P of 2.5 and 5), the complexation was found to be inefficient as noted from the significant presence of free siRNA in the gel. At N/P 7.5 and above, the siRNA encapsulation was found to be efficient (**Figure 2a**). In addition to the encapsulation efficiency, it is also necessary that we release the encapsulated siRNA molecules in the presence of a biologically relevant intracellular trigger.[34, 41] Therefore, the release of siRNA from these assemblies were assessed in the presence of a redox-stimulus at a concentration that is similar to that found in the cytosol (10 mM glutathione, GSH). In the presence of this stimulus, the siRNA release was found to be significant in the N/P 7.5 complex, but was significantly lower at higher N/P ratios (**Figure 2a**). However, dynamic light scattering (DLS) measurements revealed non-uniform, bimodal and broad particle size

distributions with poor correlation coefficients for all uncrosslinked nanoassemblies (**Figure S6a-b**) suggesting unstable nanoparticle formations.

The study of uncrosslinked complexes above provides an initial insight into the optimal N/P ratios. Note however that in our final complex, the positive charges will be removed through crosslinking. Therefore, the efficiency of siRNA encapsulation in this scenario might be very different as the balance between weakening of the complexation due to charge removal and strengthening the incarceration due to crosslinking would play an important role. To evaluate this balance, we studied the effect of crosslinking towards the formation of L-siP particles at different N/P ratios (**Figure 2b**). Upon increasing crosslinking degree, leakage of siRNA was evident from the assemblies formed at N/P 7.5 and 10. At higher N/P ratios (starting from N/P 15), in combination with higher crosslinking (0.25 equiv DTT onwards), the siRNA encapsulation was found to be stable (**Figure 2b**), as evident from narrow particle size distributions with excellent correlation coefficients. However, the release of siRNA was found to be crosslinking dependent, where the maximum release was obtained between 0.25-1 equiv of DTT crosslinking. This can be attributed to the critical balance of positive charge and crosslinking degree in L-siP nanoassemblies. At lower crosslinking degree (0-0.1 equiv DTT), residual cationic charge left after DTT treatment becomes the dominating factor and is able to hold back the siRNA tightly in the nanoassemblies. While at higher crosslinking degree (2 equiv DTT), siRNAs might be deeply buried and shielded inside the nanoassembly preventing adequate exposure to external reducing release environment. Evidently, at even higher N/P 25, where the polymeric burden was more, negligible release of siRNA was observed for similar reasons (**Figure 2b**). Based on these observations, a threshold of N/P 15 was thus considered as an efficient L-siP system for both siRNA encapsulation and release (also see later for quantification). As L-siP nanoassemblies

contain lipids, the zeta potential values were found to be negative (-30 to -40 mV, **Figure S7**) as an effect of efficient coating of DOPE and PEG- lipids.[42-43]

To further understand the complexation and release process, we also carried out CG-MD simulations (**Figure S8**). In our models, to mimic the crosslinking process, we introduced -SS- groups in the polymer assembly, while cleaving the positively charged functionalities, assuming that crosslinking has occurred. When we introduced the crosslinking in the equilibrated N/P 7.5 model system, we could clearly observe leakage of the oligos from the polymer (see **Figure S9**). Next, we built a molecular model for the more promising N/P 15 L-siP system (**Figure 2d** and **2e**). We started from an N/P 15 polymer-oligo network that was spontaneously formed in 70:30 acetone:water (v/v) via CG-MD simulation (details are available in the Computational Methods in **SI**). Then, we introduced a 100% crosslinking by adding a suitable number of DTT molecules in the system. To be sure to form a single aggregate in the center of the simulation box (useful for successful steps) following compaction due to crosslinking, we used a recently optimized simulation technique that push the system toward a single aggregation center.[44] The DTT molecules selectively and strongly interacted with the -SS- groups in the polymer during this CG-

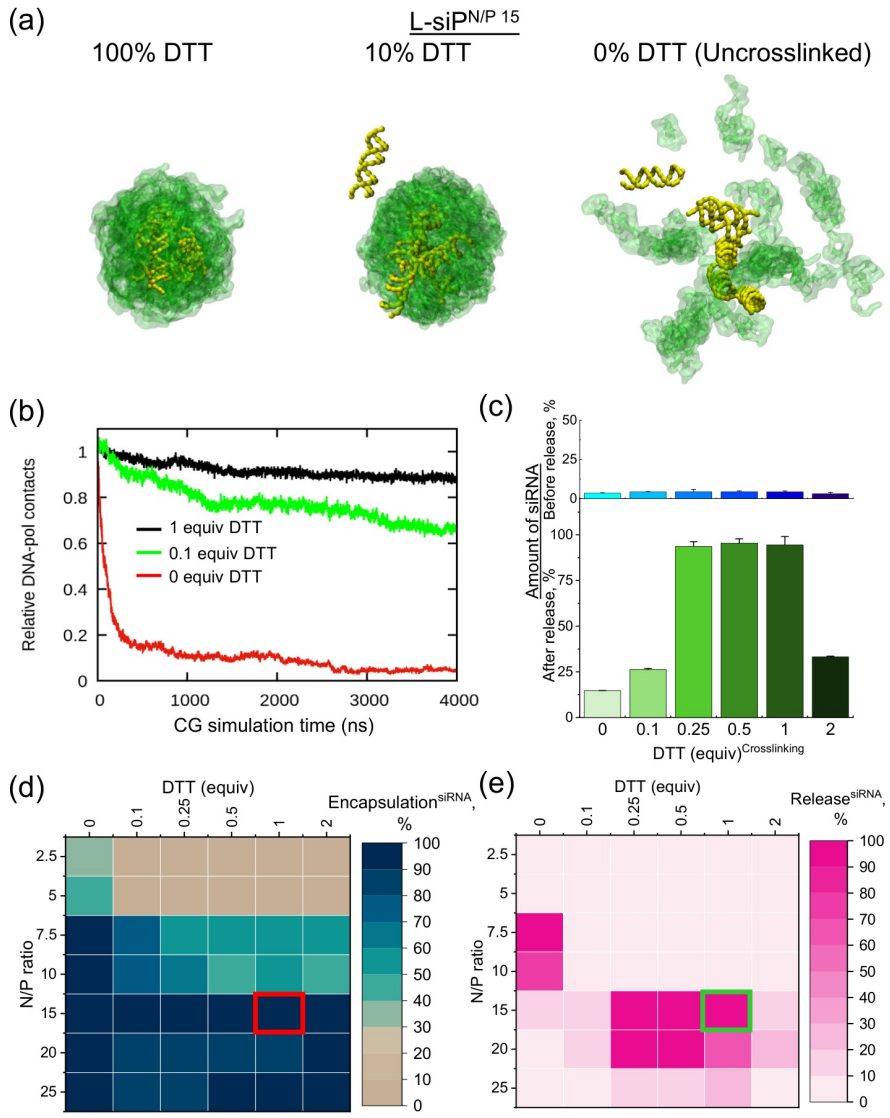

Figure 3. (a) CG-MD simulation snapshots (taken after 4 μs) showing how the oligo release proceeds at different degrees of de-crosslinking: no decrosslinking, 90% of crosslinking removed and complete de-crosslinking; (b) Quantification of the different release behaviors as the number of contacts between oligo and polymer as a function of simulation time (initial number of contacts normalized to 1); (c) Ribogreen assay to quantify encapsulated & released siRNA from L-siP$^{15/1}$; Summary of encapsulation (d) and release profiles (e) at different N/P & crosslinking ratios showing the most promising composition to be N/P 15 at 1 equiv DTT crosslinking.

MD simulation, while after coordination the cationic groups of the polymer involved in the process have been cleaved. Next, we added DOPE lipid molecules and replaced the solvent consistently with the experiments (water/organic=20, v/v). We then equilibrated the L-siP model nanoparticle

via CG-MD simulation, which provided us with an insight into the structure of this assembly at a resolution <5 Å (**Figure 2d**). The lipid layer (transparent grey) covers the interior of the assembly, where the oligos (yellow) appear as trapped in the polymer matrix (green). From the equilibrated phase CG-MD trajectory we computed the radial distribution functions of the polymer, lipid and oligonucleotides (*g(r)*: relative probability to find these in space) as a function of the distance from the center of the nanoparticle (**Figure 2e**). The superposition of the cyan and purple curves in **Figure 2e** indicates that the polymer and the oligos are uniformly mixed in the core of the assembly while the lipids cover it and constitute the shell of the nanoassembly, which resulted well stable L-siP in such experimental conditions.

Starting from this equilibrated crosslinked L-siP model, we further probed the nanoassembly to understand the effect of crosslinking on stabilization and release of oligonucleotides. Upon deleting the lipid shell, we explored the release of encapsulated oligonucleotides as a function of the de-crosslinking ratio. The polymer-oligo complex remains stable in 100% DTT, i.e., fully crosslinked condition (**Figure 3a**). However, at 90% de-crosslinking (90% of DTT molecules eliminated from the model) we observed partial release of oligoes from the assembly, which completely disassembled under complete removal of DTT (0% DTT). **Figure 3b** quantifies these observations, showing the number of contacts between the polymer and the guest oligos over time calculated with respect to the initially equilibrated nanoassembly.

We further experimentally confirmed the encapsulation and release of siRNA from the L-siP nanoparticle via RiboGreen assay for the promising N/P 15 case (**Figure 3c**, **SI**).[45] Under the encapsulated state, siRNA is significantly inaccessible to the assay reagent showing no apparent fluorescence signal generation. However, the amount of siRNA, once released from the assembly

under reducing conditions, the fluorescent signal generation was found to be dependent on the crosslink density. These observations further support the results obtained from the agarose gel retardation study above (**Figure 2a-b**). The degree of siRNA encapsulation and release obtained from agarose gel studies is summarized in **Figure 3d** and **3e**.

To further understand the fate of siRNA during encapsulation and release steps, we also performed ^{31}P NMR experiments to monitor the processes (**Figure S10**). A phosphorothioate-modified siRNA (PTsi, δ ~53 ppm) is utilized to distinguish it from the phosphorus in phosphate groups of DOPE and DSPE-PEG lipids (δ ~0 ppm).[46-47] Once encapsulated the mobility of the siRNA inside the polymer cage will be significantly impaired compared to its situation in bulk solvent. As a result, the ^{31}P band at δ ~54 ppm (for PTsi) is completely eliminated after the formation of L-siP nanoassembly, whereas it reappears upon subjecting it with the release condition (with 10 mM GSH & Triton X-100, **Figure S10**).[46] This evidence further supports the results obtained from agarose gel retardation and RiboGreen assay studies (**Figure 2a-b, 3c**). Evidently, to reduce the quantity of polymer in the L-siP assembly construction with suitable high crosslinking degree (in context of reducing cytotoxicity by shedding cationic charge), we chose the L-siP assembly (L-siP$^{15/1}$) constructed under N/P 15 with crosslinking using 1 equiv of DTT (we choose excess DTT to ensure complete removal of cationic charge as discussed in **Figure 1d**) as the desired candidate for further cellular experiments.

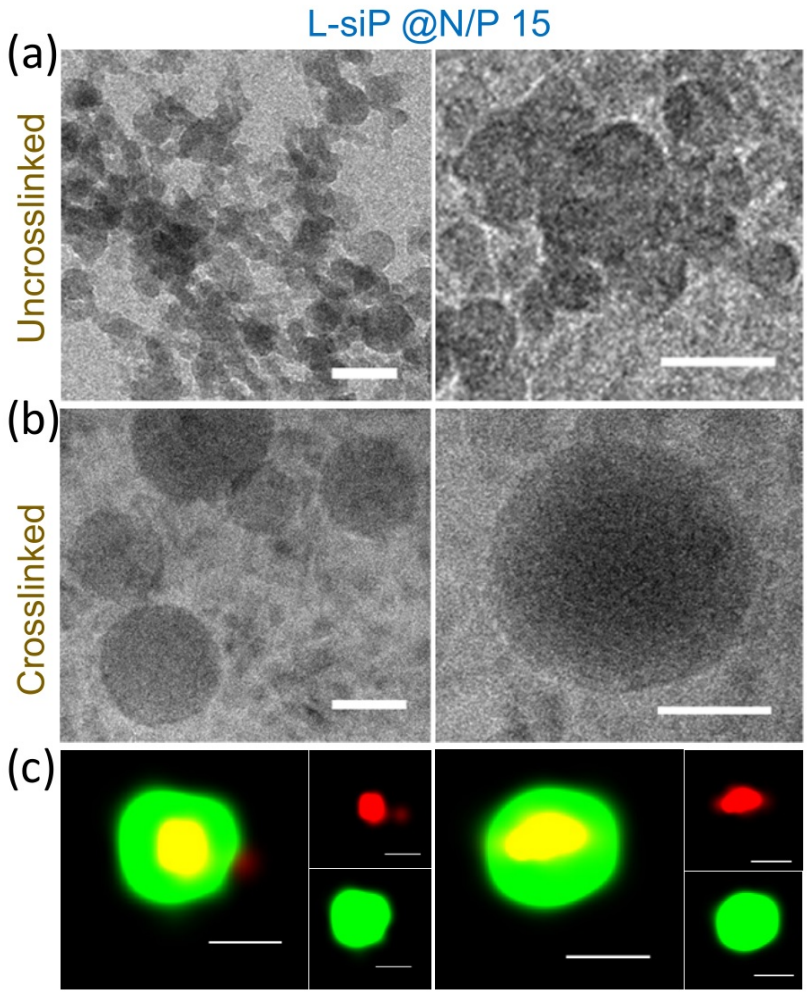

Figure 4. Cryo-TEM images of L-siP particles at N/P 15 (a) without crosslinking & (b) with cross-linking (DTT-1 equiv), scale: 50 nm; (c) N-STORM confocal microscopy images of single L-siP$^{15/1}$ particle, red: cy3-siRNA, green: carboxyfluorescein labelled DSPE-PEG lipid that coats the polymer-siRNA nanoassembly, scale: 100 nm.

3.4. Cryo-TEM and N-STORM confocal imaging of L-siP nanoassembly. Prior to evaluating the intracellular delivery of siRNA using these nanoassemblies, we further characterized the nanoassemblies via cryo-TEM and N-STORM confocal fluorescence microscopy (**Figure 4**). Cryo-TEM studies were performed for both the N/P 15 uncrosslinked and crosslinked samples. Images of the uncrosslinked assembly (**Figure 4a**) clearly show a fractal morphology consisting loose aggregates, whereas crosslinked L-siP$^{15/1}$ nanoassembly (**Figure 4b, S11**) showed uniform

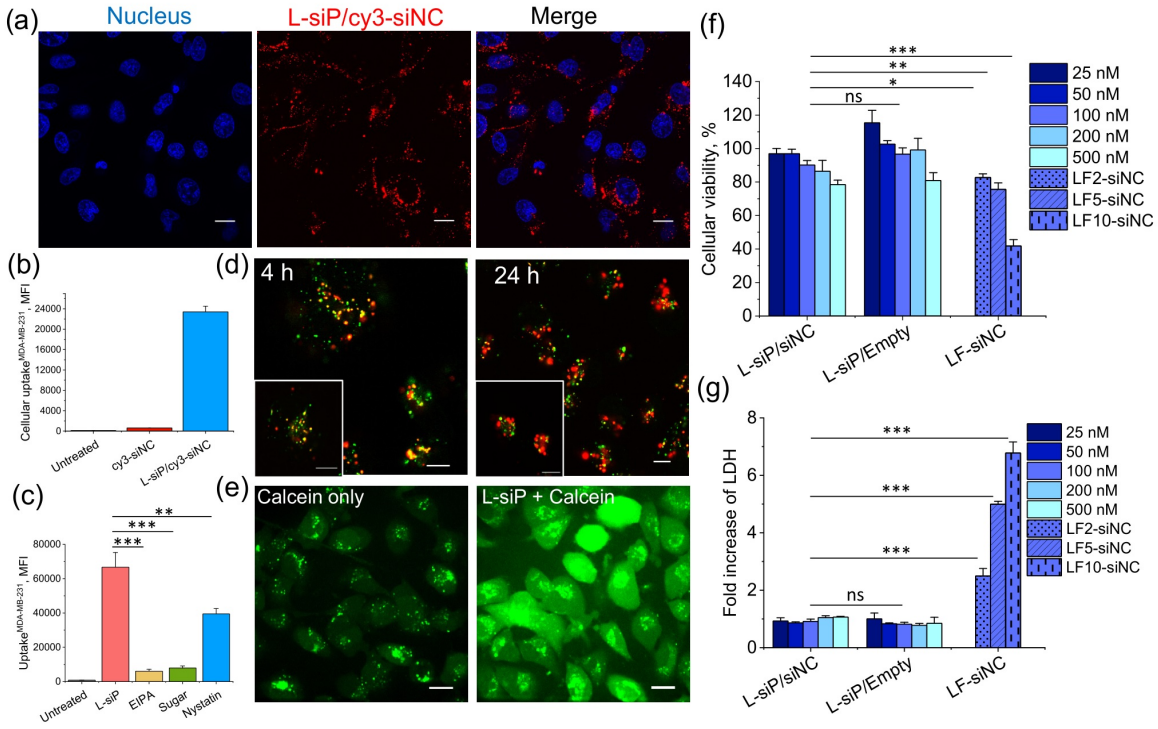

Figure 5. siRNA delivery in MDA-MB-231 cell line: (a) Cellular uptake of cy3-labelled siRNA (4 h incubation), scale: 20 µm; (b) Quantification of uptake with flow cytometry (4 h incubation); (c) Mechanism of siRNA transfection in presence and absence of endocytic inhibitors; (d) Endosomal colocalization of red cy3-siRNA and Lysotracker blue (pseudo-colored as green) after 4 h and escape after 24 h incubation, scale: 20 µm; (e) Calcein assay showing efficient escape of calcein from endosome and localization in cytosol in presence of L-siP$^{15/1}$ NA, scale: 10 µm; (f) Cellular viability and (g) LDH cytotoxicity assay for empty L-siP, L-siP nanoassemblies with different siRNA concentrations (25, 50, 100, 200 & 500 nM) at N/P 15 and Lipofectamine (LF)-siRNA complexes (with fixed 100 nM siRNA) at 2, 5 and 10 µg/mL LF concentrations; Student's t-test (compared L-siP/siNC sample bearing 100 nM siRNA with L-siP/Empty and LF samples): ***p<0.001, **p<0.01, *p<0.05, ns (non-significant)>0.05.

spherical assemblies with an average size of ~100 nm. These results are in accordance with our earlier DLS observations (**Figure 2b-c, S6**). To further characterize the particle construction, we prepared L-siP$^{15/1}$ nanoassembly utilizing carboxy-fluorescein labelled DSPE PEG-2000 lipid and cy3-labelled siRNA. As per our symbiotic self-assembly hypothesis, polymer complexed siRNA would dwell in the inner core while the shell would comprise lipid mixture surrounding the electrostatic polymer-siRNA complex. The N-STORM images in **Figure 4c** clearly demonstrate

the L-siP nanoassembly design with red cy3-siRNA comprising the inner part and green lipid layer encapsulating it externally. Interestingly, color-coded intensity profile defined by the electron scattering cross-section across the particles also matches the N-STORM measurements (**Figure 4c** & **S11**).

3.5. Cellular uptake and intracellular distribution. To test the ability of L-siP$^{15/1}$ towards intracellular delivery of siRNA, we prepared these nanoassemblies using cy3-labelled siRNA and investigated their cellular distribution in three different cancer cell lines, *viz.* mammary gland/breast cancer cell line MDA-MB-231, cervical cancer cell line HeLa and a prostate cancer cell line DU-145 (**Figure 5**, for MDA-MB-231 and **Figure S12** and **S13** for HeLa & DU-145). As shown in **Figure 5a**, a clear distribution of red fluorescence in the cytosolic region confirms efficient transfection of cy3-siRNA nanoassembly (**Figure 5b** for flow cytometry quantification). The transfection efficacy was also evaluated in HeLa and DU-145 cells though confocal laser scanning microscopy (CLSM) (**Figure S12**) and flow cytometry (**Figure S13**). A quantitative comparison reveals the following order of uptake potency in different cell lines: MDA-MB-231>HeLa>DU-145.

Next, we probed the cellular uptake mechanism via utilizing different inhibitors for endocytic pathways in the above-mentioned cell lines through flow cytometry with cy3-siRNA containing L-siP$^{15/1}$ nanoassembly (**Figure 5c** & **Figure S13**). EIPA and hyperosmolar sucrose, inhibitors for macropinocytosis and clathrin-dependent endocytosis, respectively were found to have a striking effect on uptake in MDA-MB-231 and HeLa cells, whereas the effect of nystatin, an inhibitor for caveolae-mediated endocytosis, was found to be comparatively reduced.[48-50] These results show that the major cellular internalization proceed through macropinocytosis and clathrin-

dependent pathways for MDA-MB-231 and HeLa cell lines. In contrary, DU-145 cells only showed a significant decrease in fluorescence intensity when incubated in presence of EIPA suggesting macropinocytosis being the exclusive choice of uptake pathway (**Figure S13**).

To evaluate the intracellular distribution of delivered cy3-siRNA through L-siP$^{15/1}$ assembly over time, we performed CLSM of MDA-MB-231 cells in presence of endo/lysosomal stain, lysotracker blue (pseudo-colored in green in **Figure 5d**). After 4 hours of incubation, the red fluorescence from cy3-siRNA was observed to be co-localized with lysotracker blue (**Figure 5d**), indicating that the nanoassemblies are located in endo/lysosomal compartments. Interestingly, this co-localization diminishes significantly after 24 h incubation, as indicated by clear separation of red (cy3-siRNA) and blue (pseudo-colored in green for lysotracker stain) channels suggesting endosomal disruption and release of siRNA into the cytosol. A quantitative comparison is reflected in the decrease in co-localization ratio from 0.65 (4 h) to a lower value 0.34 (24 h). The probable reason for such facile intracellular release of siRNA cargo could be explained from the fusogenicity of DOPE lipid, employed in decorating the L-siP nanoassembly, through attachment and fusion with anionic endosomal membrane.[7]

To further investigate whether endosomal disruption is indeed facilitated by L-siP nanoassemblies, we performed calcein green assay (**Figure 5e** and **Figure S14**). Calcein, a membrane-impermeable dye, shows punctate green fluorescence above its self-quenching concentration when entrapped in endo-lysosomal compartments.[51] However, the green fluorescence changes to a bright diffused pattern (dequenched state), if calcein can be released in cytosol after successful escape from endosomes mediated by delivery agents. As shown in **Figure 5e** & **S14**, the punctate green fluorescence of calcein in control cells confirms the endosomal

entrapment, whereas a diffused fluorescence is observed for L-siP$^{15/1}$ nanoassembly treated cells, suggesting efficient endosomolytic activity of the L-siP assemblies.

3.6. Evaluation of cytotoxicity and nuclease stability for L-siP$^{15/1}$. Stability of the siRNA-polyion based electrostatic complex is mostly guided by the overall high cationic charge which eventually compromises the safety of the delivery agent increasing cytotoxicity. To evaluate the safety feature of L-siP$^{15/1}$ nanoassembly, we evaluated cellular viability and plasma membrane integrity in MDA-MB-231 (**Figure 5f-g**), HeLa and DU-145 (**Figure S15**) cell lines. L-siP/siNC nanoassembly (siNC: negative control siRNA) showed ~86% cellular viability even at 200 nM siRNA concentration (with comparable polymer amount for N/P 15), whereas viability reduces to ~42% for lipofectamine-siRNA sample (LF-siNC) at an identical concentration (**Figure 5e**). Cytotoxicity study in HeLa and DU-145 cells also demonstrate a high cellular viability compared to lipofectamine (**Figure S15** & **S17**).

Next, we were interested in checking the integrity of the plasma membrane through lactate dehydrogenase (LDH) assay.[52-53] The compromised cell membrane would release cytosolic LDH enzyme into cell culture media which, in turn, can be quantified through an absorbance-based assay.[52-53] **Figure 5g** shows a minimal to no membrane damage mediated by L-siP assemblies even at a significantly high dosage (200 or 500 nM siRNA). In comparison, LF-siNC samples showed ~3 to 7-fold increase in membrane damage compared to untreated cells (**Figure 5g**, **S16** & **S17**). These results demonstrate significantly less cytotoxicity of the designed L-siP nanoassembly desirable for a safe delivery agent. As L-siP nanoassembly comprises biocompatible DOPE/PEG-based lipids and methacrylate-derived polymers, it will be prone to slow hydrolytic and enzymatic degradation under in vivo conditions with significantly less probability of systemic accumulation.[54-55]

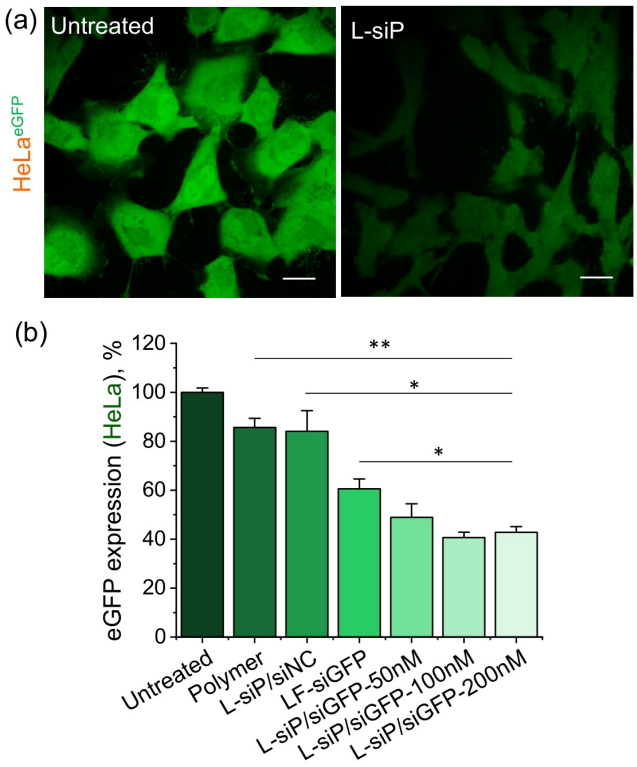

Figure 6. eGFP silencing with L-siP[15/1]: Confocal microscopy images (a) for eGFP silencing and flow cytometry data (b) for quantification of eGFP fluorescence in HeLa^{eGFP} cells; scale: 20 µm; Student's t-test: ***p<0.001, **p<0.01, *p<0.05, ns (non-significant)>0.05.

One of the bottlenecks of RNAi based technology is the limited stability of naked siRNA with a plasma half-life of <10 min due to the degradation mediated by serum endonucleases.[56] Thus, a critical requirement for an efficient delivery agent is to provide end-to-end protection till the cargo is delivered in the intracellular space. To this goal, we investigated the stability of the encapsulated siRNA in the presence of RNase A and 10% fetal bovine serum.[57-58] After incubation at different time interval with RNase A and serum, the L-siP/siNC nanoassemblies were subjected to redox-triggered release condition (10 mM GSH) and evaluated in agarose gel retardation assay. As shown in **Figure S18**, L-siP nanoassembly is efficient in protecting siRNA even after 24 h of incubation, whereas the unprotected naked siRNA is completely degraded within 4 h of incubation in presence of RNase A and serum.

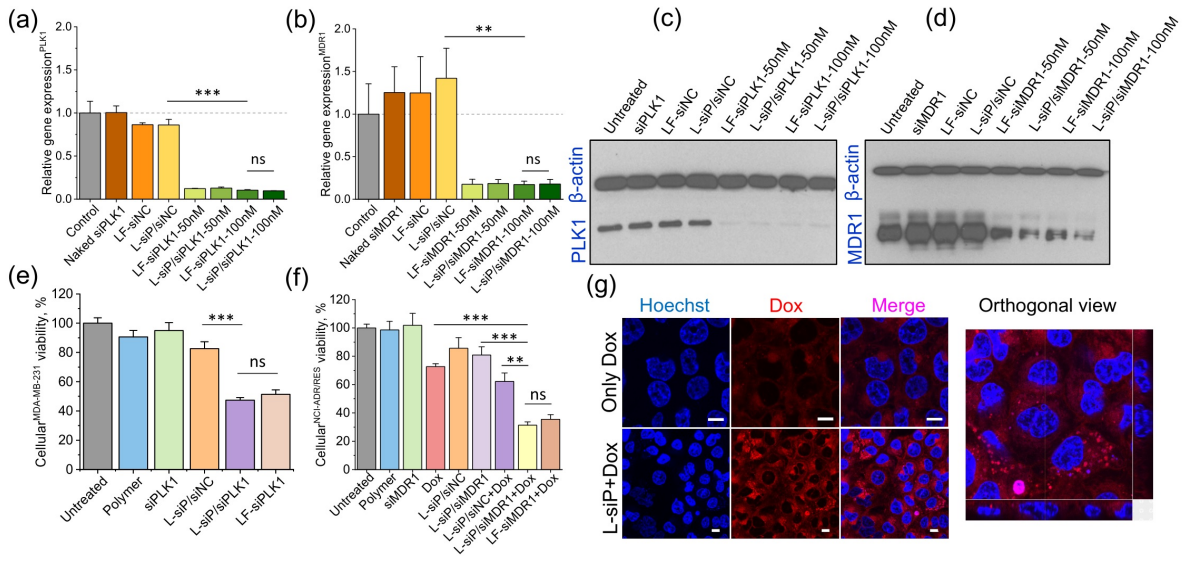

Figure 7. Gene silencing study: qRT-PCR (a, b) and western blot (c, d) analysis for (a, c) PLK1 and (b, d) MDR1; Cellular viability mediated by knock-down of (e) PLK1 gene and (f) MDR1 gene (after treatment of doxorubicin for MDR1). Uptake comparison of doxorubicin via confocal microscopy (g) in untreated and L-siP/siMDR1 treated cells; orthogonal view is for L-siP+Dox sample; scale: 10 µm; Student's t-test: ***p<0.001, **p<0.01, *p<0.05, ns (non-significant)>0.05.

3.7. Gene silencing efficacy and retrieval of cytotoxicity mediated through PLK1 & MDR1 siRNAs. Finally, we were interested in checking the efficacy of the L-siP$^{15/1}$ assembly in silencing specific gene activity. To this end, HeLa^{eGFP} and DU-145^{eGFP} cells, stably expressing eGFP, were treated with L-siP$^{15/1}$ nanoassembly containing 50, 100 and 200 nM GFP-siRNA. The reduction of green fluorescent intensity was evaluated through CLSM and flow cytometry (**Figure 6**, **S19**). CLSM images, shown in **Figure 6a** and **S19a**, reveals a clear decrease in green fluorescence intensity for both HeLa^{eGFP} and DU-145^{eGFP} cells upon treatment of L-siP$^{15/1}$ nanoassembly. Further, the GFP expression (quantified through flow cytometry, **Figure 6b** & **S19b**) was decreased to 43% at 200 nM siRNA concentration (L-siP/siGFP) in HeLa^{eGFP} cells in comparison to ~84% for negative control siRNA (L-siP/siNC) treated cells. A similar trend was also observed in DU-145^{eGFP} cells where L-siP/siGFP and L-siP/siNC treated cells showed 50% and 110% eGFP expression, respectively. Lipofectamine RNAiMAX-eGFP siRNA complex (LF-siGFP),

evaluated as positive controls, exhibited reduction of eGFP expression up to 61% and 33% for HeLa^{eGFP} and DU-145^{eGFP} cells, respectively at similar siRNA concentrations.

Encouraged by these results, we further tested the gene knock-down efficacy of the L-siP$^{15/1}$ nanoassemblies towards two other gene types, PLK1 and MDR1, through evaluation of mRNA transcription levels by quantitative real-time polymerase chain reaction (qRT-PCR) and protein expressions by western blot analysis (**Figure 7**). PLK1, a critical controller of mitosis, is found to be overexpressed in many cancer cells, leading to faster tumor progression.[59] On the other hand, MDR1 gene in multi-drug resistant cells upregulates the expression of drug transporter proteins, like P-glycoprotein (P-gp).[60] Although various small molecule inhibitors for PLK1 and MDR1 are reported in literature, siRNA-based silencing is considered to be advantageous due to its specificity, much reduced toxicity and wide applicability in multiple cancer cells. We separately constructed L-siP assemblies based on PLK1- & MDR1-siRNA and evaluated the gene knock-down efficacy in MDA-MB-231 and NCI-ADR/RES cell lines, respectively. qRT-PCR studies showed efficient silencing of both PLK1 and MDR1 genes as evident by the reduced relative gene expression levels of ~12-18% in cells treated with L-siP nanoassemblies containing PLK1 and MDR1 siRNAs (**Figure 7a** and **7b**, at 50 or 100 nM siRNA concentrations). Moreover, western blot analyses (**Figure 7c**, **7d** and **S20**) revealed that PLK1 and P-gp protein expressions were reduced to ~25% and ~31% (~24% and 51% for lipofectamine), respectively compared to untreated cells.

To further demonstrate the consequence of L-siP nanoassembly mediated siRNA delivery and gene silencing, cellular viability studies were conducted on both PLK1 and MDR1 transfected MDA-MB-231 and NCI-ADR/RES cell lines, respectively. For PLK1 compromised cells (**Figure 7e**), viability was reduced to ~47% for L-siP nanoassembly (~51% for lipofectamine positive

control). Similarly, when treated with anti-cancer drug -doxorubicin (Dox), MDR1 depleted NCI-ADR/RES cells showed mere ~31% viability compared to ~73% and ~35% for free Dox and lipofectamine transfected positive control cells, respectively (**Figure 7f**).[61] Moreover, CLSM images (**Figure 7g**) confirm significantly higher red fluorescence intensity in cells from Dox suggesting efficient penetration of the drug in L-siP nanoassembly (MDR1-siRNA) treated cells, whereas a rather subdued red fluorescence is observed for only free drug-treated cells.

4. CONCLUSION

In summary, we report a unique siRNA encapsulation and intracellular delivery approach by developing a new symbiotic self-assembly strategy of a polymer, siRNA and lipid molecules. In this approach, the initial complexation with the siRNA is made possible through classical electrostatic interactions. The key feature here is that this interaction was carried out in a relatively apolar media that not only enhances the binding affinity between the polymer and the siRNA, but also facilitates the retention of siRNA within the *in situ* generated polymer 'cage'. Note that the electrostatic complex is converted to a physically-incarcerating capsule through a crosslinking reaction, which concurrently removes the positive charge in the polymer. As the positive charges are being removed, but before the crosslinking reinforcement is fully in place, the siRNA molecules could escape the complex. However, the siRNA remains stably encapsulated, because the bulk environment of this in situ crosslinking reaction is apolar and incompatible. This structure is then finally camouflaged by the coating of a zwitterionic lipid that also imparts biocompatibility and endosomolytic ability. We call this process symbiotic, because each of these components require the other components in the solution in order to provide the final self-assembled structure.

We have rigorously characterized each of the steps in the self-assembly process, nanoassembly formation, lipid coverage, cellular internalization and cytosolic release using both experimental and computational modeling approaches. Efficient gene-silencing mediated by the designed nanoassembly provides evidence for successful integration and leverage of the built-in molecular features. We have shown that this self-assembly strategy offers several advantages: (*i*) reduction of cytotoxicity from cationic charge-based delivery vectors; (*ii*) tunability in crosslinking degree affecting siRNA binding and release efficacy; (*iii*) a biologically relevant trigger for siRNA release; (*iv*) efficient cargo protection from degradation by nucleases; and (*v*) integrated utility of the useful features of lipids (biocompatible surface & tuning endosomal escape) and designer polymers (structural integrity, multivalent interaction & protection). We anticipate that the strategy reported herein could potentially serve as a safe platform and aid in the development of RNAi based therapeutics.

ASSOCIATED CONTENT

SUPPORTING INFORMATION

The Supporting Information is available free of charge at https://pubs.acs.org

Materials & methods for characterization of polymers and L-siP nanoassembly, detailed computational methods and additional simulation data, procedures for cellular studies, cellular viability post-PLK1 and MDR1 knockdown and uptake of doxorubicin in NCI/ADR-RES cells after MDR1 knockdown experiments (PDF), N-STORM confocal video for L-siP nanoassembly (AVI).

CORRESPONDING AUTHOR

*thai@chem.umass.edu

CONFLICTS OF INTEREST

There is no conflict to declare.

ACKNOWLEDGMENT

We thank the Army Research Office (W911NF-15-1-0568) for support, NIH (T32GM008515) for CBI-training grant to KD, Dr. Jiaming Zhuang, Dr. Poulami Majumder & Piyachai Khomein for helpful suggestions & discussions, Dr. Weiguo Hu for discussions on NMR and Dr. James Chambers for help in CLSM studies. GMP and DB acknowledge the support from the Swiss National Science Foundation (SNSF grant 200021_175735 to GMP). We thank National Cancer Institute of the NIH for the NCI-ADR/RES cell line.

ABBREVIATIONS

'L-siP': 'Lipid decorated siRNA-Polymer' nano-assembly; siNC: siRNA-Negative Control; LF: Lipofectamine; PLK1: polo-like kinase-1; MDR1: multi drug resistant-1; CLSM: Confocal Laser Scanning Microscopy.

REFERENCES

1. Whitesides, G. M.; Mathias, J. P.; Seto, C. T., Molecular Self-Assembly and Nanochemistry: A Chemical Strategy for the Synthesis of Nanostructures. *Science* **1991,** *254* (5036), 1312-1319.
2. Zhang, S. G., Fabrication of Novel Biomaterials through Molecular Self-Assembly. *Nat. Biotechnol.* **2003,** *21* (10), 1171-1178.

3. Zimmermann, T. S.; Lee, A. C. H.; Akinc, A.; Bramlage, B.; Bumcrot, D.; Fedoruk, M. N.; Harborth, J.; Heyes, J. A.; Jeffs, L. B.; John, M.; Judge, A. D.; Lam, K.; McClintock, K.; Nechev, L. V.; Palmer, L. R.; Racie, T.; Rohl, I.; Seiffert, S.; Shanmugam, S.; Sood, V.; Soutschek, J.; Toudjarska, I.; Wheat, A. J.; Yaworski, E.; Zedalis, W.; Koteliansky, V.; Manoharan, M.; Vornlocher, H. P.; MacLachlan, I., RNAi-Mediated Gene Silencing in Non-Human Primates. *Nature* **2006,** *441* (7089), 111-114.
4. Li, J.; Wu, C.; Wang, W.; He, Y.; Elkayam, E.; Joshua-Tor, L.; Hammond, P. T., Structurally Modulated Codelivery of siRNA and Argonaute 2 for Enhanced RNA Interference. *Proc. Natl. Acad. Sci. U. S. A.* **2018,** *115* (12), E2696-E2705.
5. Biswas, A.; Chakraborty, K.; Dutta, C.; Mukherjee, S.; Gayen, P.; Jan, S.; Mallick, A. M.; Bhattacharyya, D.; Roy, R. S., Engineered Histidine-Enriched Facial Lipopeptides for Enhanced Intracellular Delivery of Functional siRNA to Triple Negative Breast Cancer Cells. *ACS Appl. Mater. Interfaces* **2019,** *11* (5), 4719-4736.
6. A Triumph of Perseverance over Interference. *Nat. Biotechnol.* **2018,** *36*, 775.
7. Nguyen, J.; Szoka, F. C., Nucleic Acid Delivery: The Missing Pieces of the Puzzle? *Acc. Chem. Res.* **2012,** *45* (7), 1153-1162.
8. Wang, J.; Lu, Z.; Wientjes, M. G.; Au, J. L. S., Delivery of siRNA Therapeutics: Barriers and Carriers. *Aaps J.* **2010,** *12* (4), 492-503.
9. Gallas, A.; Alexander, C.; Davies, M. C.; Puri, S.; Allen, S., Chemistry and Formulations for siRNA Therapeutics. *Chem. Soc. Rev.* **2013,** *42* (20), 7983-7997.
10. Majumder, P.; Bhunia, S.; Chaudhuri, A., A Lipid-Based Cell Penetrating Nano-Assembly for RNAi-Mediated Anti-Angiogenic Cancer Therapy. *Chem. Commun.* **2018,** *54* (12), 1489-1492.
11. Roy, R.; Jerry, D. J.; Thayumanavan, S., Virus-Inspired Approach to Nonviral Gene Delivery Vehicles. *Biomacromolecules* **2009,** *10* (8), 2189-2193.
12. Zheng, M.; Pavan, G. M.; Neeb, M.; Schaper, A. K.; Danani, A.; Klebe, G.; Merkel, O. M.; Kissel, T., Targeting the Blind Spot of Polycationic Nanocarrier-Based siRNA Delivery. *ACS Nano* **2012,** *6* (11), 9447-9454.
13. Xue, H. Y.; Liu, S. M.; Wong, H. L., Nanotoxicity: A Key Obstacle to Clinical Translation of siRNA-Based Nanomedicine. *Nanomedicine (London, U. K.)* **2014,** *9* (2), 295-312.
14. Wang, Y.; Xiao, H.; Fang, J.; Yu, X. S.; Su, Z. W.; Cheng, D.; Shuai, X. T., Construction of Negatively Charged and Environment-Sensitive Nanomedicine for Tumor-Targeted Efficient siRNA Delivery. *Chem. Commun.* **2016,** *52* (6), 1194-1197.
15. Wagner, E., Polymers for siRNA Delivery: Inspired by Viruses to Be Targeted, Dynamic, and Precise. *Acc. Chem. Res.* **2012,** *45* (7), 1005-1013.
16. Tai, W.; Gao, X., Functional Peptides for siRNA Delivery. *Adv. Drug Delivery Rev.* **2017,** *110-111*, 157-168.
17. Dunn, S. S.; Tian, S.; Blake, S.; Wang, J.; Galloway, A. L.; Murphy, A.; Pohlhaus, P. D.; Rolland, J. P.; Napier, M. E.; DeSimone, J. M., Reductively Responsive siRNA-Conjugated Hydrogel Nanoparticles for Gene Silencing. *J. Am. Chem. Soc.* **2012,** *134* (17), 7423-30.
18. Freyer, J. L.; Brucks, S. D.; Campos, L. M., Fully Charged: Maximizing the Potential of Cationic Polyelectrolytes in Applications Ranging from Membranes to Gene Delivery through Rational Design. *J Polym Sci Pol Chem* **2017,** *55* (19), 3167-3174.
19. Ripoll, M.; Neuberg, P.; Kichler, A.; Tounsi, N.; Wagner, A.; Remy, J. S., pH-Responsive Nanometric Polydiacetylenic Micelles Allow for Efficient Intracellular siRNA Delivery. *ACS Appl. Mater. Interfaces* **2016,** *8* (45), 30665-30670.

20. Shen, S. D.; Gu, T.; Mao, D. S.; Xiao, X. Z.; Yuan, P.; Yu, M. H.; Xia, L. Y.; Ji, Q.; Meng, L.; Song, W.; Yu, C. Z.; Lu, G. Z., Synthesis of Nonspherical Mesoporous Silica Ellipsoids with Tunable Aspect Ratios for Magnetic Assisted Assembly and Gene Delivery. *Chem Mater* **2012,** *24* (1), 230-235.
21. Lv, H.; Zhang, S.; Wang, B.; Cui, S.; Yan, J., Toxicity of Cationic Lipids and Cationic Polymers in Gene Delivery. *J. Control Release* **2006,** *114* (1), 100-9.
22. Hunter, A. C., Molecular Hurdles in Polyfectin Design and Mechanistic Background to Polycation Induced Cytotoxicity. *Adv. Drug Delivery Rev.* **2006,** *58* (14), 1523-1531.
23. Takae, S.; Miyata, K.; Oba, M.; Ishii, T.; Nishiyama, N.; Itaka, K.; Yamasaki, Y.; Koyama, H.; Kataoka, K., PEG-Detachable Polyplex Micelles Based on Disulfide-Linked Block Catiomers as Bioresponsive Nonviral Gene Vectors. *J. Am. Chem. Soc.* **2008,** *130* (18), 6001-6009.
24. Sizovs, A.; Xue, L.; Tolstyka, Z. P.; Ingle, N. P.; Wu, Y. Y.; Cortez, M.; Reineke, T. M., Poly(Trehalose): Sugar-Coated Nanocomplexes Promote Stabilization and Effective Polyplex-Mediated siRNA Delivery. *J. Am. Chem. Soc.* **2013,** *135* (41), 15417-15424.
25. Rosi, N. L.; Giljohann, D. A.; Thaxton, C. S.; Lytton-Jean, A. K.; Han, M. S.; Mirkin, C. A., Oligonucleotide-Modified Gold Nanoparticles for Intracellular Gene Regulation. *Science* **2006,** *312* (5776), 1027-1030.
26. Cohen, J. A.; Beaudette, T. T.; Cohen, J. L.; Brooders, K. E.; Bachelder, E. M.; Frechet, J. M. J., Acetal-Modified Dextran Microparticles with Controlled Degradation Kinetics and Surface Functionality for Gene Delivery in Phagocytic and Non-Phagocytic Cells. *Adv. Mater.* **2010,** *22* (32), 3593-3597.
27. Samarajeewa, S.; Ibricevic, A.; Gunsten, S. P.; Shrestha, R.; Elsabahy, M.; Brody, S. L.; Wooley, K. L., Degradable Cationic Shell Cross-Linked Knedel-Like Nanoparticles: Synthesis, Degradation, Nucleic Acid Binding, and in Vitro Evaluation. *Biomacromolecules* **2013,** *14* (4), 1018-1027.
28. McKinlay, C. J.; Vargas, J. R.; Blake, T. R.; Hardy, J. W.; Kanada, M.; Contag, C. H.; Wender, P. A.; Waymouth, R. M., Charge-Altering Releasable Transporters (CARTs) for the Delivery and Release of mRNA in Living Animals. *Proc. Natl. Acad. Sci. U. S. A.* **2017,** *114* (4), E448-E456.
29. Geng, Z. S.; Garren, M.; Finno, M. G., Thiabicyclononane-Based Hyperbranched Polycations for Low-Dose Oligonucleotide Delivery. *Chem. Mater.* **2018,** *30* (22), 8164-8169.
30. Cheng, Y. L.; Yumul, R. C.; Pun, S. H., Virus-Inspired Polymer for Efficient in Vitro and in Vivo Gene Delivery. *Angew. Chem., Int. Ed.* **2016,** *55* (39), 12013-12017.
31. Lu, X.; Jia, F.; Tan, X.; Wang, D.; Cao, X.; Zheng, J.; Zhang, K., Effective Antisense Gene Regulation Via Noncationic, Polyethylene Glycol Brushes. *J. Am. Chem. Soc.* **2016,** *138* (29), 9097-9100.
32. Shen, W.; Wang, Q.; Shen, Y.; Gao, X.; Li, L.; Yan, Y.; Wang, H.; Cheng, Y., Green Tea Catechin Dramatically Promotes RNAi Mediated by Low-Molecular-Weight Polymers. *ACS Cent. Sci.* **2018,** *4* (10), 1326-1333.
33. Zhang, T.; Huang, Y.; Ma, X.; Gong, N.; Liu, X.; Liu, L.; Ye, X.; Hu, B.; Li, C.; Tian, J. H.; Magrini, A.; Zhang, J.; Guo, W.; Xing, J. F.; Bottini, M.; Liang, X. J., Fluorinated Oligoethylenimine Nanoassemblies for Efficient siRNA-Mediated Gene Silencing in Serum-Containing Media by Effective Endosomal Escape. *Nano Lett.* **2018,** *18* (10), 6301-6311.
34. Ghosh, S.; Basu, S.; Thayumanavan, S., Simultaneous and Reversible Functionalization of Copolymers for Biological Applications. *Macromolecules* **2006,** *39* (17), 5595-5597.

35. Korzeniewski, C.; Callewaert, D. M., An Enzyme-Release Assay for Natural Cytotoxicity. *J. Immunol. Methods* **1983,** *64* (3), 313-320.
36. Bucur, C. B.; Sui, Z.; Schlenoff, J. B., Ideal Mixing in Polyelectrolyte Complexes and Multilayers: Entropy Driven Assembly. *J. Am. Chem. Soc.* **2006,** *128* (42), 13690-13691.
37. Akerlof, G., Dielectric Constants of Some Organic Solvent-Water Mixtures at Various Temperatures. *J. Am. Chem. Soc.* **1932,** *54*, 4125-4139.
38. Dominska, M.; Dykxhoorn, D. M., Breaking Down the Barriers: siRNA Delivery and Endosome Escape. *J. Cell Sci.* **2010,** *123* (8), 1183-1189.
39. Zhu, X.; Xu, Y.; Solis, L. M.; Tao, W.; Wang, L.; Behrens, C.; Xu, X.; Zhao, L.; Liu, D.; Wu, J.; Zhang, N.; Wistuba, II; Farokhzad, O. C.; Zetter, B. R.; Shi, J., Long-Circulating siRNA Nanoparticles for Validating Prohibitin1-Targeted Non-Small Cell Lung Cancer Treatment. *Proc. Natl. Acad. Sci. U. S. A.* **2015,** *112* (25), 7779-7784.
40. Shi, J.; Xiao, Z.; Votruba, A. R.; Vilos, C.; Farokhzad, O. C., Differentially Charged Hollow Core/Shell Lipid-Polymer-Lipid Hybrid Nanoparticles for Small Interfering RNA Delivery. *Angew. Chem., Int. Ed.* **2011,** *50* (31), 7027-7031.
41. Dutta, K.; Hu, D.; Zhao, B.; Ribbe, A. E.; Zhuang, J.; Thayumanavan, S., Templated Self-Assembly of a Covalent Polymer Network for Intracellular Protein Delivery and Traceless Release. *J. Am. Chem. Soc.* **2017,** *139* (16), 5676-5679.
42. Garbuzenko, O.; Zalipsky, S.; Qazen, M.; Barenholz, Y., Electrostatics of PEGylated Micelles and Liposomes Containing Charged and Neutral Lipopolymers. *Langmuir* **2005,** *21* (6), 2560-2568.
43. Meyer, O.; Kirpotin, D.; Hong, K. L.; Sternberg, B.; Park, J. W.; Woodle, M. C.; Papahadjopoulos, D., Cationic Liposomes Coated with Polyethylene Glycol as Carriers for Oligonucleotides. *J. Cell Biol.* **1998,** *273* (25), 15621-15627.
44. Bochicchio, D.; Pavan, G. M., Effect of Concentration on the Supramolecular Polymerization Mechanism Via Implicit-Solvent Coarse-Grained Simulations of Water-Soluble 1,3,5-Benzenetricarboxamide. *J. Phys. Chem. Lett.* **2017,** *8* (16), 3813-3819.
45. Buyens, K.; Lucas, B.; Raemdonck, K.; Braeckmans, K.; Vercammen, J.; Hendrix, J.; Engelborghs, Y.; De Smedt, S. C.; Sanders, N. N., A Fast and Sensitive Method for Measuring the Integrity of siRNA-Carrier Complexes in Full Human Serum. *J. Control Release* **2008,** *126* (1), 67-76.
46. Leung, A. K. K.; Hafez, I. M.; Baoukina, S.; Belliveau, N. M.; Zhigaltsev, I. V.; Afshinmanesh, E.; Tieleman, D. P.; Hansen, C. L.; Hope, M. J.; Cullis, P. R., Lipid Nanoparticles Containing siRNA Synthesized by Microfluidic Mixing Exhibit an Electron-Dense Nanostructured Core. *J. Phys. Chem. C* **2012,** *116* (34), 18440–18450.
47. Viger-Gravel, J.; Schantz, A.; Pinon, A. C.; Rossini, A. J.; Schantz, S.; Emsley, L., Structure of Lipid Nanoparticles Containing siRNA or mRNA by Dynamic Nuclear Polarization-Enhanced Nmr Spectroscopy. *J. Phys. Chem. B* **2018,** *122* (7), 2073-2081.
48. Majumder, P.; Baxa, U.; Walsh, S. T. R.; Schneider, J. P., Design of a Multicompartment Hydrogel That Facilitates Time-Resolved Delivery of Combination Therapy and Synergized Killing of Glioblastoma. *Angew. Chem., Int. Ed.* **2018,** *57* (46), 15040-15044.
49. Chen, Y.; Wang, S.; Lu, X.; Zhang, H.; Fu, Y.; Luo, Y., Cholesterol Sequestration by Nystatin Enhances the Uptake and Activity of Endostatin in Endothelium Via Regulating Distinct Endocytic Pathways. *Blood* **2011,** *117* (23), 6392-6403.

50. Koivusalo, M.; Welch, C.; Hayashi, H.; Scott, C. C.; Kim, M.; Alexander, T.; Touret, N.; Hahn, K. M.; Grinstein, S., Amiloride Inhibits Macropinocytosis by Lowering Submembranous pH and Preventing Rac1 and Cdc42 Signaling. *J. Cell Biol.* **2010,** *188* (4), 547-563.
51. Ren, K.; Liu, Y.; Wu, J.; Zhang, Y.; Zhu, J.; Yang, M.; Ju, H., A DNA Dual Lock-and-Key Strategy for Cell-Subtype-Specific siRNA Delivery. *Nat. Commun.* **2016,** *7*, 13580.
52. Zeller, S.; Choi, C. S.; Uchil, P. D.; Ban, H. S.; Siefert, A.; Fahmy, T. M.; Mothes, W.; Lee, S. K.; Kumar, P., Attachment of Cell-Binding Ligands to Arginine-Rich Cell-Penetrating Peptides Enables Cytosolic Translocation of Complexed siRNA. *Chem. Biol.* **2015,** *22* (1), 50-62.
53. Convertine, A. J.; Benoit, D. S.; Duvall, C. L.; Hoffman, A. S.; Stayton, P. S., Development of a Novel Endosomolytic Diblock Copolymer for siRNA Delivery. *J. Control Release* **2009,** *133* (3), 221-229.
54. van Hoogevest, P., Review - an Update on the Use of Oral Phospholipid Excipients. *Eur. J. Pharm. Sci.* **2017,** *108*, 1-12.
55. Doskocilova, D.; Mikes, F.; Pecka, J.; Kriz, J., Compositional Microstructure of Polymer Prepared by Partial Hydrolysis of Isotactic Poly(Methyl Methacrylate). *Makromol. Chem.* **1992,** *193* (10), 2529-2538.
56. Shi, B.; Abrams, M., Technologies for Investigating the Physiological Barriers to Efficient Lipid Nanoparticle-siRNA Delivery. *J. Histochem. Cytochem.* **2013,** *61* (6), 407-420.
57. Jafari, M.; Xu, W.; Pan, R.; Sweeting, C. M.; Karunaratne, D. N.; Chen, P., Serum Stability and Physicochemical Characterization of a Novel Amphipathic Peptide C6m1 for siRNA Delivery. *PLoS One* **2014,** *9* (5), e97797.
58. Wang, H. X.; Chen, W.; Xie, H. Y.; Wei, X. Y.; Yin, S. Y.; Zhou, L.; Xu, X.; Zheng, S. S., Biocompatible, Chimeric Peptide-Condensed Supramolecular Nanoparticles for Tumor Cell-Specific siRNA Delivery and Gene Silencing. *Chem. Commun.* **2014,** *50* (58), 7806-7809.
59. Jiang, Y.; Tang, R.; Duncan, B.; Jiang, Z.; Yan, B.; Mout, R.; Rotello, V. M., Direct Cytosolic Delivery of siRNA Using Nanoparticle-Stabilized Nanocapsules. *Angew. Chem., Int. Ed.* **2015,** *54* (2), 506-510.
60. Xiong, X. B.; Lavasanifar, A., Traceable Multifunctional Micellar Nanocarriers for Cancer-Targeted Co-Delivery of Mdr-1 siRNA and Doxorubicin. *ACS Nano* **2011,** *5* (6), 5202-5213.
61. Zhang, C. G.; Zhu, W. J.; Liu, Y.; Yuan, Z. Q.; Yang, S. D.; Chen, W. L.; Li, J. Z.; Zhou, X. F.; Liu, C.; Zhang, X. N., Novel Polymer Micelle Mediated Co-Delivery of Doxorubicin and P-Glycoprotein siRNA for Reversal of Multidrug Resistance and Synergistic Tumor Therapy. *Sci. Rep.* **2016,** *6*, 23859.

TOC graphic

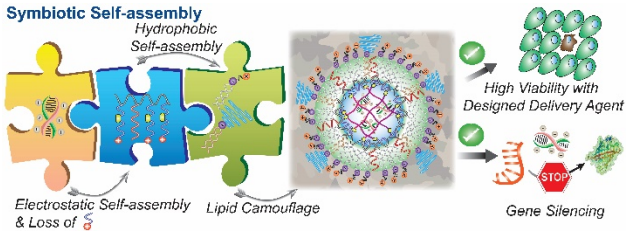
Symbiotic Self-assembly
Hydrophobic
Self-assembly
High Viability with
Designed Delivery Agent
STOP
Electrostatic Self-assembly
& Loss of
Lipid Camouflage
Gene Silencing